Magnetization, thermoelectric, and pressure studies of the magnetic-field-induced metal-insulator transition in τ-phase organic conductors

D. Graf, E. S. Choi, and J. S. Brooks
NHMFL/Physics, Florida State University, Tallahassee, Florida 32310, USA

N. Harrison
NHMFL/Los Alamos National Laboratory, Los Alamos, New Mexico 87545, USA

K. Murata
Graduate School of Science, Osaka City University, Sumiyoshi-ku, Osaka 558-8585, Japan

T. Konoike
National Institute for Materials Science, Nanomaterials Laboratory, 3-13, Sakura, Tsukuba, Ibaraki 305-0003, Japan

G. A. Mousdis and G. C. Papavassiliou
Theoretical and Physical Chemistry Institute, National Hellenic Research Foundation, Athens 116-35, Greece
(Received 11 May 2004; revised manuscript received 5 October 2004; published 24 January 2005)

We have investigated the magnetic-field-induced metal-insulator transition in the τ-phase organic conductors, which occurs in fields above 35 T and below 14 K, by magnetization, thermoelectric, and pressure-dependent transport methods. Our results show that the transition is a bulk thermodynamic process where a magnetic-field-dependent gap opens upon entry into the insulating state. We argue that the transition involves a magnetic-field-induced change in the electronic structure.

DOI: 10.1103/PhysRevB.71.045117 PACS number(s): 71.20.Rv, 72.80.Le, 71.30.+h

I. INTRODUCTION

We report magnetization, thermoelectric, and pressure-dependent transport measurements of the magnetic-field-induced metal-insulator (MI) transition in the τ-phase organic conductors τ-(*P*-(*S*,*S*)-DMEDT-TTF)$_2$(AuBr$_2$)$_{1+y}$, τ-(*P*-(*r*)-DMEDT-TTF)$_2$(AuBr$_2$)$_{1+y}$, and τ-(*P*-(*S*,*S*)-DMEDT-TTF)$_2$(AuIr$_2$)$_{1+y}$ [hereafter, τ-AuBr$_2$, $\tau(r)$-AuBr$_2$, and τ-AuI$_2$, respectively]. The MI transition has been previously reported as a rapid rise in the resistance from a metal to an insulator in the range 30–50 T at temperatures below 14 K.[1,2] The MI transition is hysteretic in field, and is also observed in magnetocaloric and skin-depth measurements. The threshold field for the MI transition (B_{MI}) is found to be nearly independent of field direction and may be driven by isotropic spin rather than Fermi surface (FS) nesting effects. Although a metallic state with Shubnikov–de Haas (SdH) oscillations is often observed below the threshold field, the resistance above the threshold field in the insulating state is immeasurable.

For τ-(*P*-(*S*,*S*)-DMEDT-TTF)$_2$(AuBr$_2$)$_{1+y}$, *P* represents the pyrazino group in the organic cation. The AuBr$_2$ linear anions reside stoichiometrically (2:1) in the square network of cations (as shown in Fig. 1) in the *ab*-conducting planes, and also nonstoichiometrically ($y \sim 0.75$) in between these molecular layers. Due to the low symmetry of the donor, and the additional interplanar anion arrangement, the unit cell is large and involves four donor layers, with crystallographic axes *a*, *b*, and $c \approx 7.3$, 7.3, and 68 Å, respectively. Materials containing one type of isomer of the donor molecule are noted by (*S*,*S*) or (*R*,*R*) in the stoichiometry, while materials with more than one type of isomer are racemic, noted by (*r*) [see Refs. 3–5 for a more detailed view of the crystal structure]. For τ-(EDO-(*S*,*S*)-DMEDT-TTF)$_2$(AuBr$_2$)$_{1+y}$ (hereafter, τ-EDO-AuBr$_2$), EDO represents the ethylenedioxy group. This material does not show a pronounced MI transition, and differs from the pyrazino compounds in other aspects, as discussed below. The ground state below 36 T in this class of materials has been studied by magnetoresistance (MR), magnetization, and pressure.[6,7] Many anomalies arise that suggest magnetic moments and magnetic memory effects occur.

The tight-binding band structure and FS is shown in Fig. 1, based on refined crystallographic studies at 290 K. An unusual feature of the electron band is the narrow, nearly dispersionless appearance. (Arita *et al.* have considered the possibility that the very flat band may lead to the appearance of magnetic properties, including the pronounced negative MR at low fields.[8]) The resulting FS has a fourfold symmetry with a single SdH frequency of about 900 T. The in-plane angular dependent MR exhibits a fourfold symmetry in high fields.[9] However, there are multiple SdH oscillations observed,[10,11] and the highest frequency F_3 is only ~500 T. Moreover, although F_3 is seen in both the pyrazino and EDO compounds, a lower frequency, $F_2 = 180$ T, with smaller amplitude than F_3 is observed for pyrazino. Three frequencies, including the lowest, $F_1 = 50$ T, are seen for τ-EDO-AuBr$_2$, where F_1 has an amplitude much larger than F_2 or F_3 in the FFT spectrum.

As discussed above, the MI transition appears to be driven by an isotropic spin (Zeeman) effect, but the temperature dependence of the phase diagram is contrary to the behavior

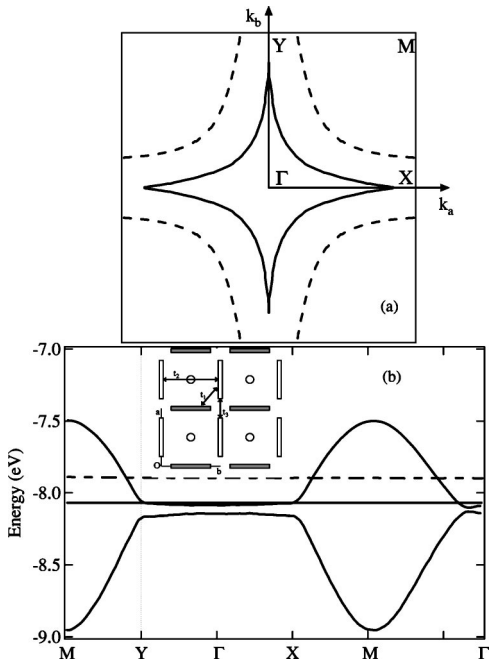

FIG. 1. (a) Star-shaped FS and (b) calculated band structure of τ-(*P*-(*S*,*S*)-DMEDT-TTF)$_2$(AuBr$_2$)$_{1+y}$ (drawn after Ref. 4). The Fermi level lies very near to the band edge. In (a) and (b), the dashed line represents $y=0$ and the solid line represents $y\sim 0.75$. The inset to (b) shows the transfer integrals between the donor molecules of the conducting *ab* plane.

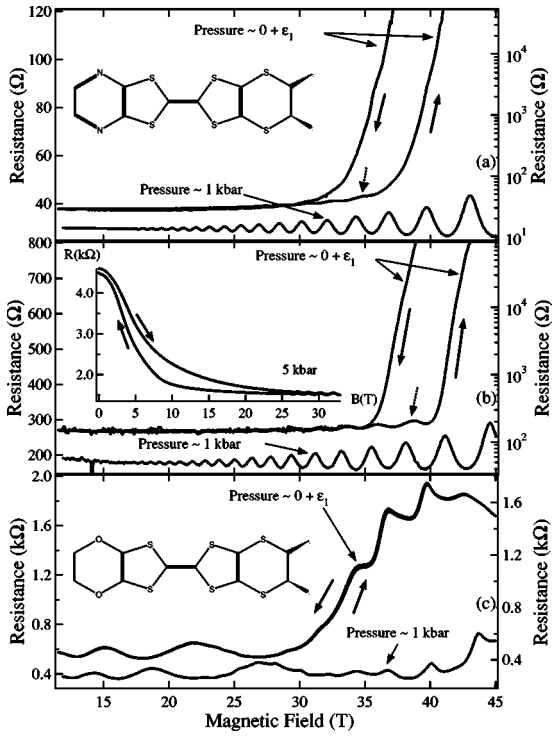

FIG. 2. Interplane resistance (R_{zz}) at $T=0.5$ K for (a) $\tau(r)$-AuBr$_2$, (b) τ-AuBr$_2$, and (c) τ-EDO-AuBr$_2$. Small pressure ε_1, left axis resistance; 1 kbar, right axis resistance. The field-induced MI transition in completely suppressed by 1 kbar, and the SdH oscillations indicate a well-defined metallic state to the maximum field. The large background MR in the case of τ-EDO-AuBr$_2$ is also suppressed by 1 kbar of pressure. The inset to (b): At lower fields, the large hysteresis, characteristic of the τ-phase materials, is observed, even under 5 kbar of pressure. The insets to (a) and (c): The τ-AuBr$_2$ and τ-EDO-AuBr$_2$ donor molecules.

of a standard charge-density-wave ground state which is removed at the Pauli limit. The transition resembles a field-induced spin-density-wave state (T_{MI} increases with field), but the transition does not follow conventional $1/\cos(\theta)$ behavior. The magnetocaloric data were highly suggestive of a thermodynamic mechanism,[1] but the nonequilibrium nature of the measurement left open questions about eddy current effects and further experiments were necessary to characterize the MI transition. For this, we have undertaken magnetization, magnetothermopower, and pressure studies.

II. EXPERIMENT

Samples were grown electrochemically by methods previously described.[12] Magnetization measurements were carried out in pulsed fields with a sample extraction susceptibility coil, and in dc fields with an AFM piezoresistive cantilever in a bridge configuration.[13,14] The cantilever is placed at the center of the magnetic field so that the response is predominantly from torque, and not gradient, forces. (A Meissner-type measurement was carried out independently at 1.7 K with a spherical lead sample to obtain an approximate calibration of the cantilever sensitivity.) Magnetothermopower studies were done in dc fields using a low-frequency digital method.[15] The pressure measurements were electrical transport in an interplanar, four-terminal configuration using gold wires and graphite paint. For pulsed field studies, a low-pressure grease encapsulation method was employed, and in dc fields a standard BeCu pressure clamp was used. Measurements were carried out at the National High Magnetic Field Laboratory: pulsed field (50 T−20 ms) experiments were done at Los Alamos, and dc fields (45 T Hybrid) were used in Tallahassee.

III. RESULTS

We first consider the MI transition as seen in electrical transport measurements under pressure and in magnetic field direction dependent MR studies. Comparisons are made between the pyrazino and the EDO compounds. This is followed by a description of magnetization measurements taken with both cantilever torque (dc field) and extraction (pulsed field) methods. Finally, we present the temperature dependence of the high-field thermopower which reveals a gap opening for fields above the MI transition.

A. Pressure dependence of the MI transition in dc magnetic fields

To explore the effects of lattice constant changes on the MI transition, pressure-dependent MR studies using a BeCu clamped cell were carried out simultaneously on three samples, $\tau(r)$-AuBr$_2$, τ-AuBr$_2$, and τ-EDO-AuBr$_2$, as shown in Fig. 2. Measurements for the "finger tight" configuration

TABLE I. Summary of the Shubnikov–de Haas oscillation frequencies for $\tau(r)$-$AuBr_2$, τ-$AuBr_2$, and τ-EDO-$AuBr_2$. Where the temperature dependence of the SdH was measured, the effective-mass parameter, m^*/m_0, is given in parentheses after the SdH frequency.

Pressure	Frequency	τ-(r)-$AuBr_2$	τ-$AuBr_2$	τ-EDO-$AuBr_2$
ε_1	F_1			47.3
1 kbar	F_1			58 (1.97)
ε_1	F_2		166	175
1 kbar	F_2	185 (4.75)	185 (4.45)	200 (2.14)
ε_1	F_3	497	505	465
1 kbar	F_3	494 (7.66)	507 (7.80)	484 (3.94)
5 kbar	F_3		537	

of the pressure cell showed behavior very similar to previous studies. Here the samples are encapsulated in the pressure fluid, but there is no further compression of the fluid at room temperature. Hence, the pressure at low temperatures is nearly zero, but indeterminate, i.e., $P=0+\varepsilon_1$.[16] The MI transition typical of all pyrazino compounds was observed in $\tau(r)$-$AuBr_2$ and τ-$AuBr_2$, as was the large background MR in the τ-EDO-$AuBr_2$ sample above 30 T. SdH oscillations were also seen in all three materials. However, under a pressure of only 1 kbar, the MI transition in the pyrazino was completely suppressed, and SdH oscillations persisted to the highest fields. Likewise, the MR background in the EDO sample was dramatically reduced. (The MR background will be discussed in more detail below.) Note the low-field hysteresis of the negative MR persists [inset, Fig. 2(b)], even at 5 kbar, well above the threshold pressure needed to suppress the MI transition. Under these same conditions, changes in the SdH frequencies were observed where τ-$AuBr_2$ showed a 6% increase above measurements at lower pressures. For convenience, we provide a summary of SdH frequencies and associated effective masses for these materials in Table I.

The racemic material exhibited SdH oscillations for small pressure ($0+\varepsilon_1$ kbar) which previously had not been observed in this variant of the pyrazino family in dc or pulsed field MR under ambient pressure [Fig. 2(a)]. The Dingle temperature of the τ-$AuBr_2$ sample is lower than for the racemic $\tau(r)$-$AuBr_2$, which is consistent with the more disordered nature of the racemic material. Using the Dingle temperature to estimate the relaxation time, τ ($T_D = h/4\pi^2 k_B \tau$), and the fundamental oscillation frequency (F_3) to estimate the Fermi velocity, ν_F, we obtain a mean free path of 170 Å at $T=0.5$ K for the racemic sample. From the simple Drude picture, the zero field in-plane resistance yields a mean free path of the order of the unit cell (10 Å). Hence, although the temperature-dependent resistivity suggests a "bad metal," the quantum oscillations show metallic character.

B. Pulsed magnetic field studies—Pressure effects in the pyrazino compound

The high sensitivity of the MI transition to pressure, which is completely suppressed by 1 kbar, is difficult to explore with the standard pressure clamp system. Therefore, a grease encapsulation method was used to apply a small pressure ($0+\varepsilon_2$ kbar) below 1 kbar.[16] (This also avoided eddy current problems associated with BeCu clamped pressure cells that arise in pulsed fields.) The MR was studied in a 50 T pulsed magnet, as shown in Fig. 3. The sample, first measured without the grease, showed the characteristic abrupt change at the MI transition accompanied by transients in the signal, as previously reported.[1] When the sample was measured under identical conditions, but with the grease pressure, the threshold field increased at a rate in the range of $\approx 10-100$ T/kbar. With pressure, the transient effects were reduced, indicating a corresponding decrease in the insulating behavior. The low-pressure study therefore confirmed the extreme sensitivity of the MI transition to pressure.

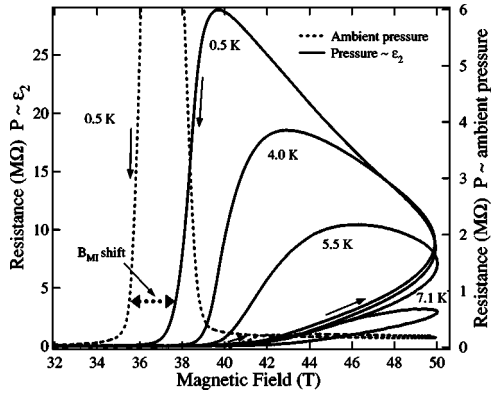

FIG. 3. Low-pressure study of the field-induced MI transition in the $\tau(r)$-$AuBr_2$ material in pulsed fields at 0.5 K. Dashed line: ambient pressure signal, solid lines: ε_2 bar pressure signal for different temperatures. The thin, solid arrows represent the direction of the field sweep while the thick, dotted arrow shows the pressure-dependent shift for the down-sweep.

C. Pulsed magnetic field studies—Angular dependent effects in the EDO compound

Although there is no dramatic MI behavior in the EDO material, there is a background MR that appears above 30 T. Since in the pryazino compounds the MI transition is nearly independent of field orientation,[1] we carried out angular dependent MR measurements on the EDO system to examine the behavior of this background. Our results are shown in Fig. 4(a) for pulsed magnetic fields at low temperatures for different field orientations. We find that the background MR above 30 T is present in the $B\|c$ ($\theta=0°$, where θ is the angle between the applied field and c-axis) data, and it remains, even for the $B\|ab$ plane ($\theta=90°$) orientation where no SdH oscillations appear. This indicates that there is a contribution to the MR in the EDO material that is independent of FS topology. The background MR increases significantly (although not as dramatically as the MI transition in the pyrazino systems) above 30 T. Since the SdH oscillation amplitude is proportional to the background MR, in Fig. 4(b) we have plotted the same results versus inverse perpendicular field [$B\cos(\theta)$], where we have normalized the $\theta=0°$, 30°, and 60° data by dividing out the $\theta=90°$ background

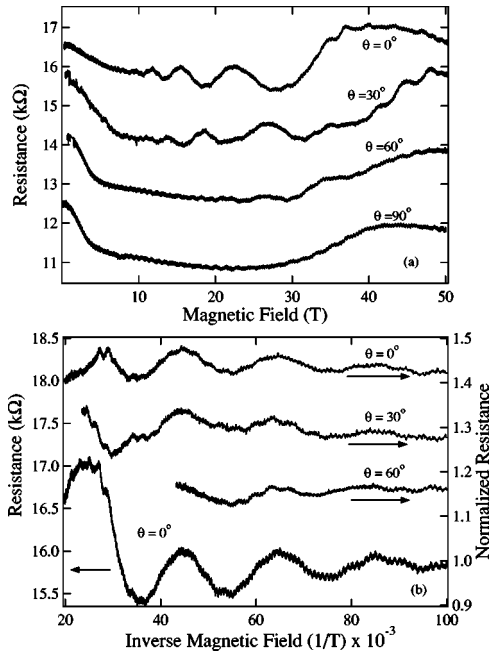

FIG. 4. The angular dependent MR of the τ-EDO-$AuBr_2$ system at 0.5 K in pulsed fields. All traces are offset for clarity. (a) MR data for different field orientations. (b) Left axis: 0° data without normalization vs inverse field. Right axis: Oscillatory MR vs $1/B\cos(\theta)$ normalized to the background MR from the 90° data in panel (a). See text for discussion.

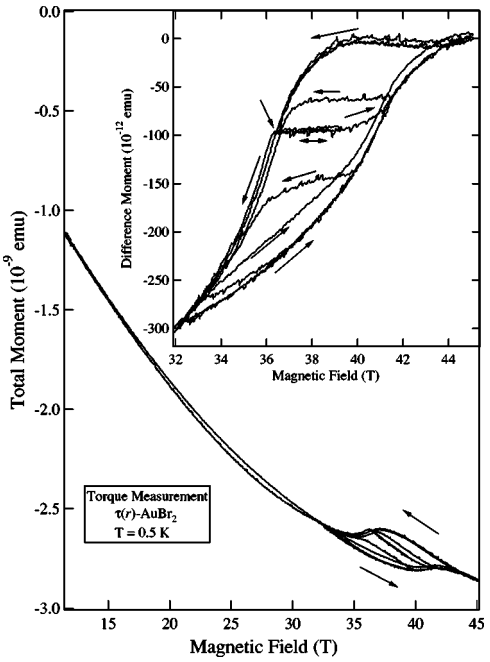

FIG. 5. Cantilever torque magnetization signal from $\tau(r)$-$AuBr_2$ at 0.5 K. The overall background signal depends on the orientation of the cantilever with respect to field. The inset shows detailed behavior of the hysteresis in the magnetization in the field-induced MI transition region. The arrows indicate the direction of the field sweep. The double arrow indicates reversible behavior between the upper and lower threshold limits.

MR. For comparison, we also show the $\theta=0°$ data in Fig. 4(b) without normalization. If we focus on the low-frequency (50 T) SdH oscillation, it is clear that its amplitude above 30 T deviates significantly from standard Lifshitz-Kosevich theory, since the amplitude is much larger than the $\exp(-T/B)$ dependence. However, upon normalization with the background MR, the final oscillation falls into the $\exp(-T/B)$ description. Hence we conclude from this study that there is an isotropic background MR which rises significantly above 30 T in the EDO system which is not part of the SdH signal.

D. Magnetization

To test the thermodynamic nature of the MI transition in the pyrazino materials, we carried out two complementary studies of the magnetization. In Fig. 5, we present the torque magnetization signal for a τ-**(***P*-(*r*)-DMEDT-TTF**)**$_2$$(AuBr_2)_{1+y}$ single crystal at 0.5 K mounted on an AFM-type cantilever. The overall change in the background signal with field is characteristic of the sample+cantilever response, which can change sign with different orientations in field.[17] However, the behavior of the hysteretic envelope above 35 T remains the same for all measurements. This behavior, shown in the Fig. 5 inset, is the signature of the MI transition in the magnetization. Of note, within the magnetization envelope that defines the hysteretic MI transition region, the signal appears reversible for increasing and decreasing fields. Since cantilever measurements are well suited for the measurement of the relative, but not the absolute moment, we have further quantified this change in magnetization by employing the extraction method in pulsed magnetic fields at 0.46 K, as shown in Fig. 6. Here the difference in the integrated sample-in and sample-out signals is shown versus the magnetic-field up-sweep. The magnetization, which increases linearly with magnetic field (paramagnetic), shows a slight increase in slope above 30 T. This further rise in magnetization is indicated as the deviation from linearity plotted against the right scale. The sizes of the total magnetization signals are in reasonable agreement, even with the difficulties in obtaining an absolute calibration for the very small samples on the cantilever and the correspondingly small moment changes observed.

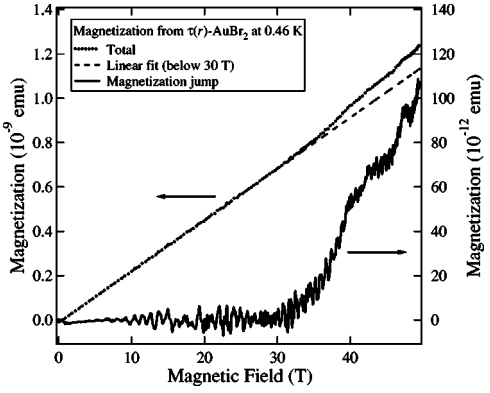

FIG. 6. Magnetization of $\tau(r)$-$AuBr_2$ at 0.46 K from a sample extraction susceptibility coil system in a pulsed field magnet.

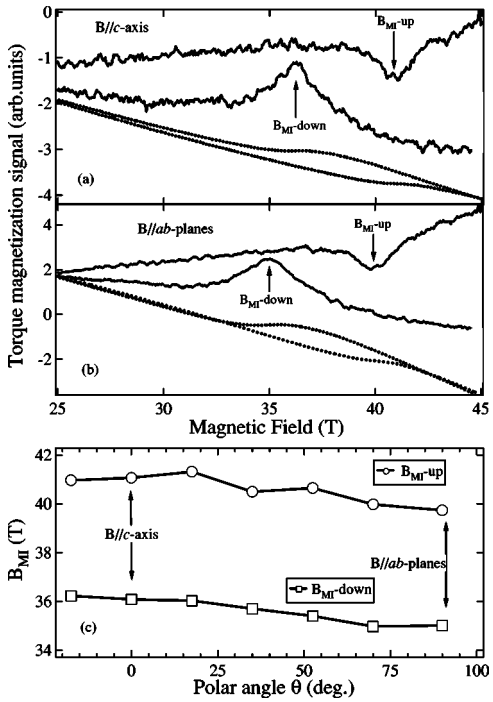

FIG. 7. Cantilever torque magnetization signal from $\tau(r)$-$AuBr_2$ at 0.5 K vs field orientation. Threshold fields are determined from the peak in the derivative of the signal at the hysteretic field-induced MI transitions. (a) $B\|c$ axis: magnetization signal (dashed lines), derivative of signal (solid lines). (b) $B\|ab$ planes: magnetization signal (dashed lines), derivative of signal (solid lines). (c) Field orientation dependence of hysteretic threshold fields B_{MI}-up and B_{MI}-down for full angular range.

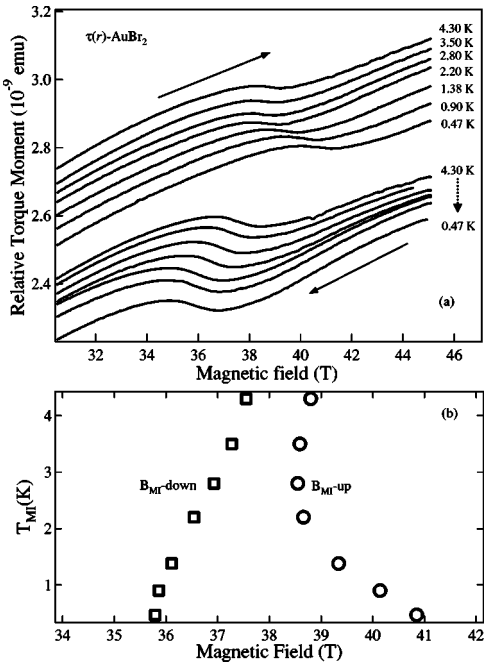

FIG. 8. Cantilever torque magnetization signal from $\tau(r)$-$AuBr_2$ for $B\|c$ vs temperature. (a) The up-sweep and down-sweep traces for each temperature have been offset to show the temperature dependence of the threshold field regions for B_{MI}-up and B_{MI}-down, respectively. Solid arrows indicate the direction of field sweep. (b) Summary of the phase diagram for T_{MI} vs B_{MI}. The threshold fields were determined from the peaks in the derivatives of the traces, as indicated in Fig. 7. The increase in B_{MI}-up at lower temperatures is consistent with previous transport and magnetocaloric studies.

The signature of the field-induced MI transition was further explored through the angular and temperature dependence of the magnetization in dc fields. In Fig. 7(a), we show the total magnetization for the field perpendicular to the conducting layers ($B\|c$ axis) and in Fig. 7(b) parallel to the conducting layers ($B\|ab$ planes). To mark the hysteretic transition field thresholds (B_{MI}-up and B_{MI}-down), we have used the peaks in the derivative of the signal, as indicated in Figs. 7(a) and 7(b), and a complete plot of the angular dependence of the threshold fields is shown in Fig. 7(c). The temperature dependence of the magnetization at the MI transition is shown in Fig. 8(a), where we have separated the up and down sweeps to highlight the different behavior of the two branches. We have used the derivatives of the signals (as in Fig. 7) to obtain the threshold fields, which are presented in Fig. 8(b) versus in a T-B phase diagram. The low-temperature appearance of the MI phase diagram is in good agreement with that obtained by transport, skin depth, and magnetocaloric measurements. This includes the behavior of the high-field phase boundary which has a negative dT/dB slope for $T\rightarrow 0$.

E. Magnetothermopower study of the MI transition

Magnetothermopower measurements for τ-**(**P-(S,S)-DMEDT-TTF**)**$_2(AuI_2)_{1+y}$ were carried out in constant dc fields versus temperature as shown in Fig. 9. The inset of Fig. 9 shows the zero field temperature dependence. τ-AuI_2 is isostructural to the other pyrazino compounds and exhibits the same high-field insulating state.[1]

We first discuss the zero-field thermopower data, where several points should be noted. (i) The sign of the thermopower is negative, which is consistent with the Hall effect measurement results on τ-$AuBr_2$.[10,18] (ii) The temperature dependence shows a broad maximum at around 50 K, below

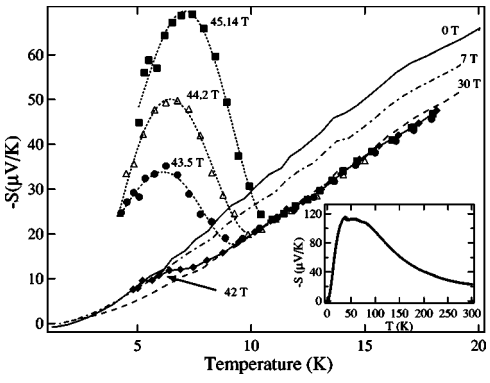

FIG. 9. Magnetothermopower measurements for τ-AuI_2 carried out in constant dc fields vs temperature in the region of the field-induced MI transition. Inset: zero-field thermopower vs temperature.

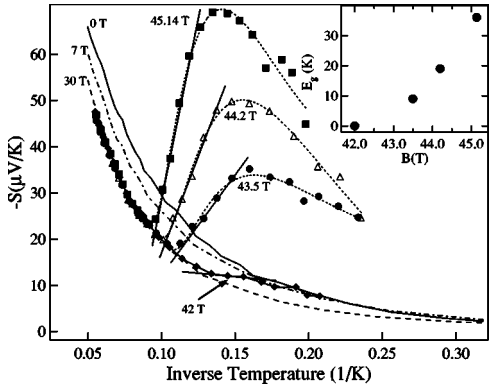

FIG. 10. $S(T)$ vs $1/T$ representation of magnetothermopower measurements in the field-induced MI regime. Lines are fits to the activated behavior below the transition for each field. Inset: Field dependence of the activation energy.

which thermopower shows normal metallic behavior, i.e., decreases to zero almost linearly. This behavior is often observed in the in-plane thermopower of many two-dimensional organic conductors.[19] Merino *et al.* suggested that the peak in S(T) can be explained by the destruction of the Fermi liquid quasiparticles, resulting in a "bad" metal.[20] In this model, a smooth crossover from coherent Fermi liquid excitations at low temperatures to incoherent excitations at high temperatures leads to a nonmonotonic temperature dependence in transport properties. The slope of the metallic thermopower region of τ-AuI_2 is large compared to other organic conductors,[20] indicating a small bandwidth, or large density of states at the Fermi level. We will return to this important point in the discussion section. The ratio of Coulomb repulsion to small measured bandwidth (U/W) would be large, revealing a tendency towards an insulating state, as seen in MR measurements. (iii) Recalling the anomalous upturn in the resistance of the τ-$AuBr_2$ and τ-AuI_2 compounds[3,11] for $T \rightarrow 0$, the thermopower in the same region shows no anomalous behavior. Since thermopower is extremely sensitive to changes of electronic properties, but is rather insensitive to disorder, it is likely that anomalous behavior observed in the zero-field resistance measurement may be due to disorder inherent in this material.

In the magnetothermopower, the MI transition for $B > B_{MI}$ is clearly seen as an abrupt increase in S below the transition temperature T_{MI}. Upon further cooling, the thermopower decreases again, showing a broad peak. At lower temperatures, it was impossible to measure the thermopower signal since the sample impedance was too high and exceeded the range of the nanovoltmeters.

If we focus the thermopower behavior just below T_{MI}, the increase of thermopower can be explained as the opening of an energy gap in the insulating state. In Fig. 10, the data are presented to show the slope of S versus 1/T below T_{MI}, which is a measure of the activation energy gap, E_g. Since S(T) is proportional to the temperature dependence of the transport conductivity σ through $\ln[\sigma(T)]$, S(T) can be expressed as $S(T) \sim E_g/T$ and E_g, determined in this manner, is shown in the inset of Fig. 10. The energy gap opens at around B=42 T and it increases with magnetic field.

The broad peak in thermopower below T_{MI} has also been observed in other organic conductors,[21] where the MI transition temperature is high enough so that the lower temperature behavior can be observed. This behavior may be due to carriers from impurities or defect levels that become important when the band carrier density decreases below the impurity/defect density.

IV. DISCUSSION

The field-induced MI transition is a general feature of the pyrazino τ-phase materials. All measurements to date, including electrical transport, skin depth, magnetocaloric effect, magnetization, susceptibility, and thermopower, show that for many different pyrazino samples, there is a bulk, field-induced, hysteretic transition from a metallic state to an insulating state. Although the temperature dependence of the phase boundary is similar to that seen in the field-induced spin-density-wave (FISDW) states in the Bechgaard salts, there is little evidence that the MI transition involves FS nesting since the MI transition is only slightly dependent on field direction. Moreover, in the FISDW phases the conductivity remains finite, whereas in the pyrazino τ-phase materials it vanishes along all crystallographic directions,[1] and there is no evidence for imperfectly nested FS pockets remaining, as is generally the case in a FISDW system. In this discussion, we consider several possible mechanisms that could either lead to, or strongly influence, the field-induced MI transition.

The present work reveals that the MI transition is thermodynamic, and from the value of the magnetization change we estimate that the transition involves an itinerant-to-localized transformation of about 10^{17} electrons/cm^3. Indeed, this change in carrier concentration is not far from that involved in the MI transition in, for instance, doped-semiconductor systems. The thermopower measurement further confirms the thermodynamic nature of the transition, since it shows that a field-dependent energy gap opens above the MI transition.

In these materials, field-induced changes in electronic structure of order 10 meV or less could cause a catastrophic change, including a gap opening at the Fermi level. The tight-binding electronic structure indicates that the bandwidth below the Fermi energy (see Fig. 1) is relatively shallow, of order 10 meV, and the band is very flat. Zero-field thermopower measurements are consistent with this narrow bandwidth. The thermopower measurement also sets the relevant energy scale for the MI transition: the MI activation energy is field-dependent, and reaches $E_a=3$ meV by 45 T (note $\Delta=2E_a$). The other energy scales include the Fermi energy, the Zeeman band splitting, the Landau spectrum, and broadening due to disorder. If we consider a field of 40 T, and the largest (F_3) orbit, then $g\mu_B B=4.6$ meV, $(\hbar eB/m^*)=0.6$ meV, $E_F=\hbar eF/m^*=8.4$ meV, and $T_D=0.1$ meV, respectively. Due to the smaller values, the Landau gap and disorder probably do not strongly affect the MI transition. Rather, the bandwidth, E_F, E_a, and the Zeeman energy appear to be the competing energy scales.

A simple model which would produce a field-dependent energy gap is where the flat conduction band shifts relative to

TABLE II. Band-structure calculation results for different samples of the pryazino and EDO compounds studied by XRD. Directions of t_1, t_2, and t_3 given in the inset to Fig. 1(b). See text for discussion.

Compound	Crystal No.	t_1 (meV)	t_2 (meV)	t_3 (meV)	Method
EDO	1	206	24	2	EHT
EDO	2	184	16		EHT
Pyrazino	3	138	16		EHT
EDO	1	96.2	0.1	4.6	VBHF
Pyrazino	3	78.2	0.2	6	VBHF

the Fermi level with increasing field. However, although the spin-down band will increase, the spin-up band will decrease in energy, and this cannot produce an insulating state if the Fermi level remains fixed. Experimentally we do not see evidence for spin-split Landau levels, nor is there any indication of a change in the SdH frequency at the entry into the MI phase. [Even a careful investigation of the SdH structure on the rapidly rising resistance signals at the MI transition, in Fig. 2(a) for instance, shows that it is not shifted in frequency or phase from the SdH waveform in the lower field fully metallic phase.]

There are three other important factors in the behavior of the MI transition. The first is that it is highly suppressed in the EDO materials. The second is that the MI transition is hysteretic, indicating coupling between the electronic and lattice structures. The third is the very high sensitivity of the MI transition to pressure. Differences in the behavior of the pyrazino and EDO materials may result from small variations between these structures. The asymmetric donor molecules are arranged in a square lattice where each nearest-neighbor donor has an opposite orientation [noted by the shaded and unshaded rectangles of the *ab* plane in the inset to Fig. 1(b)]. Using the crystallographic data from several crystals of the pryazino and EDO compounds at room temperature,[4,22] the electronic band-structure calculations by extended Huckel tight-binding (EHT)[4,22] and valence bond Hartree-Fock (VBHF)[22,23] methods have been performed. Both methods and both materials give a star-shaped Fermi surface. The values of the transfer integrals are given in Table II. The t_1 term is the largest interaction in every case. It is also larger for EDO than pryazino in each type of calculation. Hence, it is possible that the pyrazino materials are more susceptible to perturbations in high magnetic fields. Since this would depend on atomic or molecular orbitals, and not the FS topology, the field interaction could be relatively isotropic. If the magnetic field altered the coordination near or at the *N-S* coupling sites slightly, it would change the electronic structure, and it would be coupled to the lattice. Two nearly equivalent molecular configurations could give rise to the hysteretic behavior. The apparent reversibility *within* the hysteresis loops in Fig. 5, coupled with the widening of the hysteresis region at low temperatures, suggests a double-well process which is thermally activated. Previous magnetocaloric studies are also indicative of this kind of two-state switching, and also show the widening of the hysteretic region at low temperatures. The high sensitivity of the MI transition to pressure further supports the role the lattice plays in the close proximity of the MI and metallic phases.

The observation of a field-induced MI transition in complex organic materials is not without precedent. The Q2D organic superconductor, κ-(BEDT-TTF)$_2$Cu[N(CN)$_2$]Cl, also shows a field-induced MI transition in MR. The unit cell involves two donor layers, and the anion structure is sometimes referred to as "polymeric."[24] Moreover, in this class of κ-(ET) salts, there is variable configurational order in the ethylene groups that affects both the superconducting transition and the appearance of SdH oscillations.[25–27] The nonmetallic state measured in κ-(BEDT-TTF)$_2$Cu[N(CN)$_2$]Cl has been described in terms of loosely bound molecules that are susceptible to small perturbations of external parameters.[28] Given that the τ-phase materials have a four-donor-layer repeat unit cell, combined with a complex, nonstoichiometric anion structure, a similar sensitivity to perturbations can be expected.

The coupling of the magnetic field to the electronic structure may involve an enhanced susceptibility. Previously, Arita *et al.*[8] have considered the flat band character of the electronic structure where it is argued that the magnetic susceptibility is enhanced due to the flatness of the bands along k_x and k_y. It would be instructive to examine tight-binding band-structure calculations where we could explore the Zeeman and diamagnetic effects of high magnetic fields on the molecular orbitals, since the field dependence of the electronic structure could be estimated. Likewise, structural probes including Raman, ultrasonics, or even x-ray diffraction would be very useful to gauge the role of the lattice at the transition.

ACKNOWLEDGMENTS

This work is supported by NSF-DMR 02-03532, and the NHMFL is supported by a contractual agreement between the NSF and the State of Florida. D.G. is supported through a GK-12 Fellowship. We are grateful to H. Yoshino for helpful discussions.

[1] J. S. Brooks, D. Graf, E. S. Choi, L. Balicas, K. Storr, C. H. Mielke, and G. C. Papavassiliou, Phys. Rev. B **67**, 153104 (2003).

[2] D. Graf, L. Balicas, J. S. Brooks, C. Mielke, and G. C. Papavassiliou, Int. J. Mod. Phys. B **16**, 21 (2002).

[3] G. C. Papavassiliou, K. Murata, J. P. Ulmet, A. Terzis, G. A. Mousdis, H. Yoshino, A. Oda, D. Vignolles, and C. P. Raptopoulou, Synth. Met. **103**, 1921 (1999).

[4] J. S. Zambounis, J. Pfeiffer, G. C. Papavassiliou, D. J. Lagouvardos, A. Terzis, C. P. Raptopoulou, P. Delhaes, L. Ducasse, N. A.

Fortune, and K. Murata, Solid State Commun. **95**, 211 (1995).
[5] G. C. Papavassiliou, G. A. Mousdis, A. Terzis, C. P. Raptopoulou, K. Murata, T. Konoike, and Y. Yoshino, Synth. Met. **120**, 743 (2001).
[6] H. Yoshino, T. Konoike, K. Murata, G. C. Papavassiliou, T. Sasaki, T. Yamamoto, and H. Tajima, Mol. Cryst. Liq. Cryst. Sci. Technol., Sect. A **376**, 171 (2002).
[7] T. Konoike, A. Oda, K. Iwashita, T. Yamamoto, H. Tajima, H. Yoshino, K. Ueda, T. Sugimoto, K. Hiraki, T. Takahashi, T. Sasaki, Y. Nishio, K. Kajita, G. C. Papavassiliou, G. A. Mousdis, and K. Murata, Synth. Met. **120**, 801 (2001).
[8] R. Arita, K. Kuroki, and H. Aoki, Phys. Rev. B **61**, 3207 (2000).
[9] J. S. Brooks, L. Balicas, K. Storr, B. H. Ward, S. Uji, T. Terashima, C. Terakura, J. A. Schlueter, R. W. Winter, J. Mohtasham, G. L. Gard, G. C. Papavassiliou, and M. Tokumoto, Mol. Cryst. Liq. Cryst. Sci. Technol., Sect. A **380**, 109 (2002).
[10] K. Storr, L. Balicas, J. S. Brooks, D. Graf, and G. C. Papavassiliou, Phys. Rev. B **64**, 045107 (2001).
[11] T. Konoike, K. Iwashita, H. Yoshino, K. Murata, T. Sasaki, and G. C. Papavassiliou, Phys. Rev. B **66**, 245308 (2002).
[12] G. C. Papavassiliou, D. J. Lagouvardos, I. Koutselas, K. Murata, A. Graja, L. Ducasse, and J. P. Ulmet, Synth. Met. **86**, 2043 (1997).
[13] E. Ohmichi and T. Osada, Rev. Sci. Instrum. **73**, 3022 (2002).
[14] D. Graf (unpublished).
[15] E. S. Choi, J. S. Brooks, J. S. Qualls, and Y. S. Song, Rev. Sci. Instrum. **72**, 2392 (2001).
[16] A SPG10 (semiconductor pressure gauge) was used from the High Pressure Research Center of the Polish Academy of Sciences, Warszawa, Poland. The gauge indicated a positive pressure well below 1 kbar (at the lower end of the calibration range of the gauge) in both frozen *N*-grease and Daphne oil. Manganin wire resistance was also measured in the Daphne oil from which we estimate a pressure of 10–100 bar.
[17] D. Graf, E. S. Choi, J. S. Brooks, M. Matos, R. T. Henriques, and M. Almeida, Phys. Rev. Lett. **93**, 076406 (2004).
[18] N. Fortune, K. Murata, G. C. Papavassiliou, D. J. Lagouvardos and J. S. Zambounis, in *Electrical, Optical, and Magnetic Properties of Organic Solid State Materials*, edited by A. F. Garito, A. K.-Y. Jen, C. Y.-C. Lee, and L. R. Dalton, MRS Symposia Proceedings No. 328 (Materials Research Society, Pittsburgh, 1994), p. 307.
[19] E. S. Choi, J. S. Brooks, and J. S. Qualls, Phys. Rev. B **65**, 205119 (2002), and references therein.
[20] J. Merino and R. H. McKenzie, Phys. Rev. B **61**, 7996 (2000).
[21] K. Mortensen, E. M. Conwell, and J. M. Fabre, Phys. Rev. B **28**, 5856 (1983).
[22] G. C. Papavassiliou, D. J. Lagouvardos, J. S. Zanbounis, A. Terzis, C. P. Raptopoulou, K. Murata, N. Shirakawa, L. Ducasse, and P. Delhaes, Mol. Cryst. Liq. Cryst. Sci. Technol., Sect. A **285**, 83 (1996); G. C. Papavassilou (unpublished).
[23] F. Castet, A. Fritsch, and L. Ducasse, J. Phys. I **6**, 583 (1996); L. Ducasse (private communication).
[24] J. M. Williams, J. R. Ferraro, R. J. Thorn, K. D. Carlson, U. Geiser, H. H. Wang, A. M. Kini and M.-H. Whangbo, *Organic Superconductors (Including Fullerenes)* (Prentice Hall, Englewood Cliffs, NJ, 1992).
[25] T. F. Stalcup, J. S. Brooks, and R. C. Haddon, Phys. Rev. B **60**, 9309 (1999).
[26] M. A. Tanatar, T. Ishiguro, H. Ito, M. Kubota, and G. Saito, Phys. Rev. B **55**, 12 529 (1997).
[27] T. Ishiguro, K. Yamaji, and G. Saito, *Organic Superconductors II* (Springer-Verlag, Berlin, 1998).
[28] Y. V. Sushko, H. Ito, T. Ishiguro, S. Horiuchi, and G. Saito, J. Phys. Soc. Jpn. **62**, 3372 (1993).